International Journal of Innovative Research and Reviews, 6(2) 113-120

International Journal of Innovative Research and Reviews
ISSN: 2636-8919
Website: www.injirr.com
doi:
Research paper, Short communication, Review, Technical paper

RESEARCH ARTICLE

A Numerical Simulation and Aerodynamic Investigation of Air Flow around Supersonic Airfoil Profiles

Muhammet Kaan YEŞİLYURT[1] Mansur MUSTAFAOĞLU[2] İlhan Volkan ÖNER[2,*]

[1] *Department of Machinery and Metals, Vocational College of Technical Sciences, Ataturk University, Erzurum, Turkiye*
[2] *Department of Mechanical Engineering, Faculty of Engineering, Ataturk University, Erzurum, Turkiye*

** Corresponding author E-mail: ivoner@atauni.edu.tr*

ARTICLE INFO

Received : 11.02.2022
Accepted : 12.08.2022
Published : 12.15.2022

Keywords:
Supersonic Airfoil
Numerical simulation
Aerodynamic coefficients
Elastic
ANSYS fluent

ABSTRACT

In this study, flow field analysis was performed to determine the aerodynamic coefficients for the SC36210 and NACA0018 airfoil profiles in supersonic compressible flow at 2 Mach. During this analysis, ANSYS Fluent, and geometric modeling was used. Numerical simulation of flow was made by K-ω Transition turbulence model. Change in the attack angle versus the divergence angle of airfoil surface profile was examined for elastic flexible SC series. According to the results, as the Mach number of the free flow increases, the aerodynamic coefficient values decrease. In addition, Elastic flexible airfoil profiles for use in supersonic wings have higher performance advantages compared to SC36210 and NACA0018 series airfoils.

Contents

Cite this article Yeşilyurt MK, Mustafaoğlu M, Öner İV. A Numerical Simulation and Aerodynamic Investigation of Air Flow around Supersonic Airfoil Profiles. *International Journal of Innovative Research and Reviews (INJIRR)* (2022) 6(2) 113-120
Link to this article: http://www.injirr.com/article/view/125

1. Introduction

Fluid Structure Interaction (FSI) problems can be simulated thanks to the advancements in the computer technology and development of numerical methods. While computational fluid dynamics (CFD) code is required to solve FSI problems, computational structural dynamics (CSD) code is used to solve aerodynamic forces and determine the deformations in solid models. The force created by the fluid motion on the structure will affect the deformation that will occur on the structure and this process will continue in a cyclic manner. Each computational solver codes are developed with different numerical methods. While the CFD is based on the Finite Volume method (FVM), the CSD method is based on the Finite element method (FEM). Improving the aerodynamics of flying objects in different flight conditions is one of the most important issues in the aviation industry and is being studied by many researchers today. Airfoils are designed to provide the highest efficiency and optimum performance to flight conditions [1]. Smart deformation in the airfoil configuration improves the aerodynamic performance of the aircraft, in other words, the deformable airfoils adapts to the variable flight conditions and produces a specific configuration for each flight condition. Variable flight conditions suggest that a single configuration that can improve aerodynamic efficiency and maneuverability is not possible [2, 3]. Elastic airfoil profile, will significantly improve the performance of future aircraft. A fundamental issue here is that the structure (airfoil) is strong enough not to deform under aerodynamic forces, while it has the flexibility to deform elastically [4].

Smart deformability can be actively controlled, that is, no unpredictable deformation occurs in the airfoil body. This will allow the aircraft to change the configuration of its airfoils smartly according to specific flight conditions. An airfoil that can be deformed under flight conditions can increase the lift-drag ratio by 10 to 20 percent [5]. Historically, problems in various aspects such as cost, complexity, and weight, were experienced with deformable airfoils, as a result of which no significant progress could be recorded in these airfoils to date. Recent advances in smart materials have overcome many of these problems [6, 7].

For the verification of the FSI problem, the AGARD 445.6 airfoil model, which has experimental and computational data available in the literature, was implemented. Yates Jr. [8] examined and reported the fluttering phenomenon for the AGARD 445.6 model with experimental results. In addition, various articles have been published after detailed studies on this topic [9–15]. Furthermore, the FSI problem for the airfoil, which was mentioned in the article published by Goud et al. in 2014, was simulated at 0.9 Mach number, and the pressure and turbulent kinetic energy values on the airfoil were obtained [16].

The use of smart materials, which is the basic mechanism of deformable airfoils, has made many advances in this area today [17]. Many studies have been carried out in this area because of the advantages of elastic airfoils. Tai and Lim [18] numerically investigated the effect of active elasticity in beam direction on buoyancy and thrust in three different airfoil types. The results showed that the efficiency increased by up to 76% by choosing the escape edge as the center of curvature. Hariri [19] investigated the effect of two dimensional unstable viscous flow around elastic objects by numerically examining the effect of beam direction elasticity on upper and lower airfoils. The results showed that both input power and output power increased in the elastic state, but the ratio of output power to input was higher.

The main purpose of this study is to better understand the aeorelasticity theory, to analyze airfoil aeroelasticity, to determine the flapping speed for the selected airfoil profile by using aeroelastic methods with computational fluid dynamics methods. For this purpose, further information was obtained about the advanced use of FLUENT program, the structure-fluid interaction solver was examined and the sample solver was created. The concept of flapping, which is defined as the dynamic instability problem occurring in the aircraft during flight, has been tried to be interpreted and the methods existing in the literature have been investigated for solving thereof. The results obtained were compared with the studies in the literature and verified. In terms of engineering, the purpose of the study is to calculate the critical flapping speed with easy yet precise methods and accordingly to determine the design requirements in order to prevent flapping, which is extremely dangerous for aerospace vehicles.

2. Material and method

Fluid-structure interaction is a type of interconnected problem that examines the interdependence of fluid and mechanical structures. The behavior of the flow depends on the shape and movement of the structure, and the deformation of the structure depends on the forces applied by the fluid on the structure. The fluid and structure interaction occurs in a variety of fields including engineering, medicine, and even in daily life. This interaction will be even more important when the interdependence of action and reaction is severe. The pumping of blood to the ventricles by the human heart with the opening and closing of the heart valves is a clear example of fluid-structure interaction.

Fluid-structure interaction plays an important role in engineering applications and is very influential in design decisions. Due to its non-linear nature and interaction of fluid and structure being time-dependent, the use of analytical methods to solve such problems is very difficult and sometimes impossible. Analytical solution is possible only in a few cases where simple and acceptable solutions of partial equations can be reached by simple assumptions. Before getting into the simulation of these problems, it is a must to recognize the fundamental equations for such problems.

These equations describe the physics under study and often appear in the form of partial equations. On the one hand, the famous Navier-Stokes equations, which are the main equations of the fluid mechanics, and the governing equations of the structure derived from the general theory of elasticity need to be solved on the other. In most cases, these equations are simplified by using models (e.g. turbulence models, wall functions, linear elastic materials, etc.) or the complexity of the equations are reduced by using hypotheses/assumptions, such as incompressible fluid, inviscid fluid, small strain, etc. [20].

2.1. Fluid equations

Navier-Stokes compressible fluid equations are the main equations of fluid mechanics. First, these equations are written in the usual way, then the same equations are written in the form of a traditional O'Leary algebra to generalize the equations to the fluid-structural interaction problem.

To solve the governing equations in the fluid part, the Spalart-Allmaras turbulent model was used. This turbulent model is a single equation model that solves a modeled transition equation for turbulent dynamic viscosity (ν_t) fluid flow. The boundary is subject to reverse pressure gradients. The final transfer equation of the Spalart-Allmaras model is as follows:

$$\frac{D\tilde{\nu}}{Dt} = c_{b1}\tilde{S}\tilde{\nu} + \frac{1}{\sigma}[\nabla.((\nu+\tilde{\nu})\nabla\tilde{\nu}) + c_{b2}(\nabla\tilde{\nu})^2] - c_w f_w \left[\frac{\tilde{\nu}}{d}\right]^2 \quad (1)$$

Steady-state and compressible Navier-Stokes equations are as follows. Due to the transient sound regime of the flow regime and the perceptibility of heat transfer, the energy equation is considered together with the continuity and momentum equations, which are given below separately.

Continuity equation:

$$\frac{\partial\rho}{\partial t} + \nabla.(\rho V) = 0 \quad (2)$$

Momentum Equation:

$$\frac{\partial(\rho V)}{\partial t} + \nabla.(\rho VV) = -\nabla P + \nabla.[\mu(\nabla V + \nabla V')] + F \quad (3)$$

Energy conservation equation:

$$\frac{\partial(\rho E)}{\partial t} + \nabla.[V(\rho E + P)] = \nabla.(k\,\nabla T) + \Phi \quad (4)$$

$$\Phi = \left[\mu\left(\frac{\partial v_i}{\partial x_j} + \frac{\partial v_j}{\partial x_i}\right) + \delta_{ij} + \lambda\nabla V\right]\frac{\partial v_i}{\partial x_j} \quad (5)$$

2.2. Traditional Lagrange-Euler method for fluid-structure interaction problems

When simulating FSI problems, it is an important point to consider choosing the type of kinematic description of the flow field so that the boundaries can move and deform.

The Arbitrary Lagrangian–Eulerian (ALE) method is suitable for solving such problems. ALE is intended to make use of powerful sides of both Lagrangian and Eulerian descriptions of motion, while minimizing the drawbacks of the two. As a combination of both, ALE provides high accuracy in defining moving boundaries and helps solve the problem of large distortion in the presence of moving boundaries.

Figure 1 should be given a randomly determined motion in order to achieve a continuous zoning capability. Because of this effect of freedom, offered by the ALE definition, in moving the computational mesh, the larger distortions of the continuum can be resolved with greater resolution than the purely Euler approximation can provide, which is more than Lagrange method would allow. The simple example in Figure 2 illustrates the ability of the ALE description to accommodate significant deviations of the computational mesh while maintaining the clear definition of interfaces that are entirely unique to the Lagrange approach.

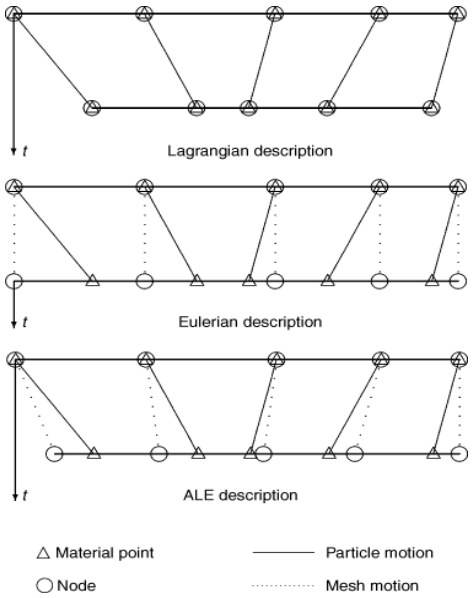

Figure 1 One-dimensional example of Lagrangian, Eulerian and ALE descriptions for mesh and particle motion [21]

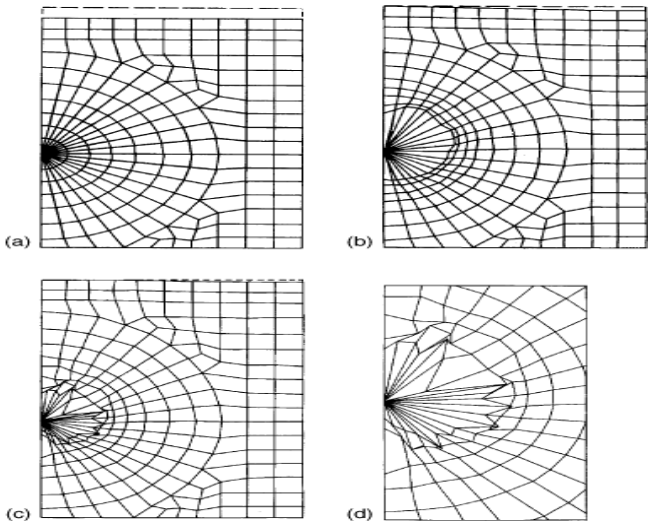

Figure 2 Lagrangian and ALE descriptions: (a) initial FEmesh ; (b) ALE mesh at t = 1 ms ; (c) Lagrangian mesh at t = 1 ms ; (d) Interface details in the Lagrangian description [21].

When mesh configurations obtained with ALE description (with automatic continuous zoning) and Lagrangian description were compared, the Lagrangian approach can be seen to be a disruption of the computational mesh, in contrast to the ability of the ALE approach maintain a highly ordered mesh configuration.

2.3. Boundary conditions

2.3.1. Flow boundary conditions

Figure 3 shows the boundary conditions applied. Since the deformation in the airfoil profile did not cause any bending along the length, all simulations were carried out in 3 dimensions to be more realistic. According to Figure 3, the left area shows the input current, the right area shows the output current and the change in the airfoil profile. Other assumptions are given in Table 1.

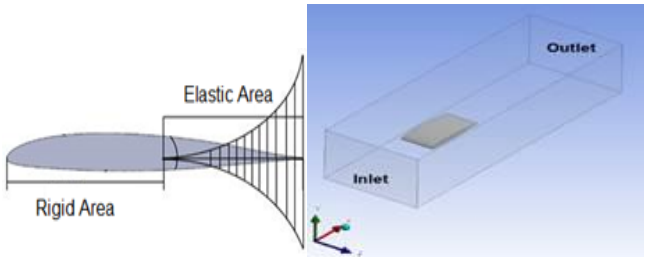

Figure 3 Geometry to be analyzed and boundary conditions applied

Table 1 Physical properties of the model

Property	Value
Airfoil profile chord length (mm)	100
Air Specific heat capacity (j / kg.K)	287
Ratio of Specific heats (γ)	1.5
Mach number	2
Air speed (m/s)	686.4
Air temperature (K)	283.15

2.3.2. Elastic boundary conditions on the fin

As shown in Figure 3, the elastic deformation at the attack and escape edge occur as the air flow passes, and by the forces applied to the attack and escape edge, a large and parabolic external load which is applied to predetermined elastic parts with uniform changes.

$$T.E.Load = -F_{back}\left(\frac{x}{l}\right)^2 load\left(\frac{t}{dt}\right) \quad (6)$$

In this equation, *l* is ferroelastic lengths edge. Wherein F_{back} is the maximum intensity of load at the attach and escape edge, which decreases as getting closer to the rigid part in the middle of the airfoil profile. Due to the increase in aerodynamic forces on the escape edge, the force applied in this part is higher than the attack edge. If the elastic forces fall below certain values, the aerodynamic forces will prevail the elastic forces, making the simulation difficult, and as a result, unstable deformation will occur. Therefore, it is necessary to choose the amount of elastic force that is to be applied to produce the desired deformation.

$$sin\alpha_t = \frac{\delta_{TE}}{c} \quad (7)$$

$$m = \frac{\delta_{TE}}{2*c} \quad (8)$$

In these equation, c is the airfoil profile beam, m is the airfoil profile camber with respect to the beam, the angle of deviation or displacement of the escape and attack edge, and αt is the angle of the radius. By combining Equations (7) and (8), the displacement of the escape edge and the attack edge can be obtained as follows:

$$\delta_{TE} = c\left(m + \frac{\alpha_t}{2}\right) \quad (9)$$

3. Numerical analysis

3.1. Finite Element Method

The finite element method is an excellent and powerful method for solving engineering problems. As known, there are different methods to solve an engineering problem, such as testing, analytical solution, etc. However, analytical solutions are sometimes not possible for complex engineering problems and also tests are very expensive yet cannot be carried out for every problem. However, when the finite element method is mastered and used correctly, many problems can be investigated using it. In fact, this method does not have any limitations and even if a commercial software cannot solve a particular problem, it is still possible to code and advance in solving the problem. Therefore, this method is a very good and powerful method that all researchers in the field have to learn. This method solves problems easily and provides good and acceptable results with high accuracy. Of course, this software requires not only operational knowledge, but also engineering knowledge. Boundary conditions and loads on the element must be specified correctly. It is clear that an incorrect output will be obtained if wrong input is given to finite element software.

3.2. Steps to perform finite element analysis

Finite element method, all the engineering model is broken down into smaller parts called finite elements, and the solution is achieved by solving the problem for these finite elements. Each element itself consists of nodes to which input and output values are assigned. Each element is represented by a linear (first order) or nonlinear (which can be second order or higher) shape function. When analyzing a finite element model, the number of equations is so large that some models reach more than 20,000 equations.

All these equations must be solved together in order to reach the solution. The number of these equations directly depends on the number of nodes and elements placed in the model. The user must have an insight about the description of the problem in order to build the model and mesh according to the type of problem, degrees of freedom of the model, boundary conditions, initial conditions, etc. The steps for performing an analysis with finite element software are as follows:

- Defining the problem, choosing the element type, choosing the system of units and determining the properties of the materials.
- Creating a geometric model, determining the grid size and meshing the model.
- Application of geometric, static, thermal and load constraints.
- Solving the problem and viewing the results.

3.3. Coupled-field analysis

Coupled-field analysis is used in problems where two or more domains have interference phenomena (coupled). Examples of such analysis are: thermal stress analysis, thermoelectric analysis and fluid-structure analysis. Two methods can be used to perform this analysis:

3.3.1. Indirect (sequential) method

This method, includes two or more sequential analyses, uses a separate area for each analysis. For example, in the heat stress analysis, the results of the heat distribution on the model are first calculated in the first analysis. Then, in the second analysis, which is a structural analysis, the results of the heat distribution in the form of volumetric loading (temperature) are applied to the model and the problem is

solved under this loading. This method is used in problems where coupling fields does not involve high-order nonlinear interventions. In this case, two (or more) analyses can be performed separately. For example, in the same example, the thermal stress can be first performed in a tentative thermal analysis and then the temperature of each node can be loaded at any time in any loading step, or in the second analysis conducted on the same node, and the results of the thermal stress can be obtained.

3.3.2. Direct method

This method usually involves an analysis where the problem of coupling the interference of different fields is addressed and the elements used in this method have all the degrees of freedom required for the analysis known as fasteners. This method is used in problems where the interference of problem fields has a high degree of linearity.

Computational fluid dynamics (CFD) is used to solve problems which are difficult to solve with the basic equations of fluid mechanics theory, by using numerical methods and algorithms. Open source codes and software packages are available for CFD. CFD creates a mesh structure that consists of small and simple elements and nodes that simulate the differential equations of the flow, and reaches the solution step by step through these small elements by iterations. This process, which is performed in computer environment, gives very realistic results when correct analysis inputs are given.

CFD is a suitable solution method for complex flow problems, however in order for the creation of numerical meshing, and for defining and interpreting boundary layer and realistic conditions, it requires literature knowledge, and experimental data as well as experience. Due to the complexity of aeroelastic problems, the computer environment is an important tool for simulating the problem. For aeroelasticity, fluid mechanics codes alone are insufficient. Since the structural deformation is very important, the solution is preferred to be reached by solving the fluid and structure codes in combination, which can be called Computational Aeroelasticity.

3.4. FSI Method

While different methods have advantages over one another, the two-way coupling solution is generally more accurate particularly for larger deflections where the fluid field is strongly influenced by structural deformation. With one-way coupling simulation, one can enjoy significantly lower computational time due to that the deformation of the fluid mesh does not need to be calculated as it provides a constant quality mesh, but only a strong two-way coupling, which can be of second-order time accuracy and are more stable, can guarantee energy conservation at the interface [22].

4. Results and discussion

A numerical solution to a problem requires a proper mesh. An unorganized triangular mesh was used in this study. Since we are dealing with a FSI problem, it is clear that the mesh created will change during the solution of the problem. Therefore, by choosing an unorganized mesh, there will be more flexibility in the computational mesh and the convergence of the problem will not be a big issue. For a better comparison of the results obtained, the number of components used in all simulations (rigid and elastic state) was set as 6,254,000. Figure 4 and Figure 5 show quality and validation of mesh. Owing to the use of Lagrangian-Eulerian method in the solution of the problem, the distortion in the mesh after the deformation of the airfoil profile was very little. Figure 4 shows the mesh around the airfoil profile before deformation. To investigate computational mesh independence, the diagram was examined in different mesh numbers and the results showed that the computational mesh was independent (Figure 5).

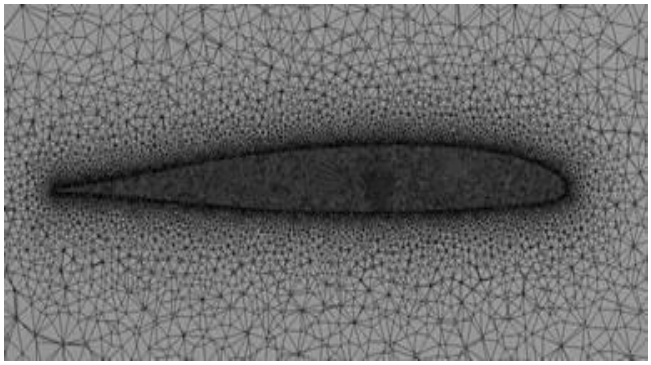

Figure 4 Mesh construction

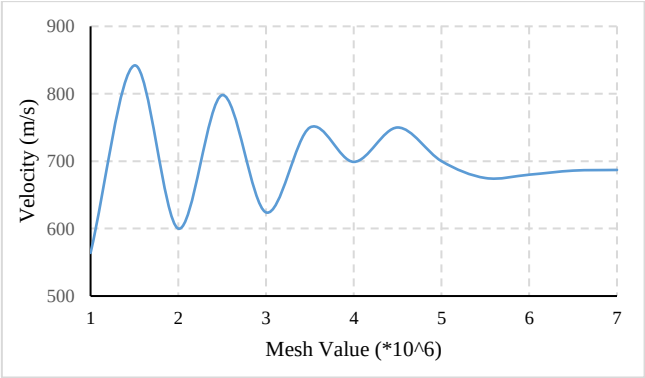

Figure 5 Mesh independence analysis scheme for different mesh numbers

In this study, a comparison was made between the flow separation in elastic airfoil profiles. To do so, the shear stress values of the walls above and below the airfoil profile were calculated using the following equation.

$$\tau_w = \mu\left(\frac{\partial u}{\partial y} + \frac{\partial v}{\partial x}\right)/2 = \mu\epsilon \quad (10)$$

where ϵ is the strain tensor.

Starting point of the separation on the elastic airfoil profile is shifted backwards with Malim deformation. There is a significant time delay in flow separation. For example, at a 5-degree attack angle, the stagnation point appears at 0.25 beam, while this point for airfoil profiles is at 0.1 beam. For smaller angles of attack, this significant difference is gradually eliminated and hence airfoil elasticity will have little effect on the separation area.

According to Figure 6, Figure 7 and Figure 8, when only the zero-degree angle considered, in rigid state, it can be seen that the flow behaviors in the top and bottom of SC36210

and NASA0018 airfoil profiles were similar due to the symmetry of the profile, and that no compression difference was created. The gradual deformation of the profile eliminates the symmetry creating a pressure difference on the upper and lower sides of the airfoil due to the asymmetry. As the angle of divergence or the intensity of the deformation increases, the pressure differential of the force increases, thus the upper side pressure decreases and the lower side pressure increases. As the upper side pressure decreases, the velocity of the flow in this area increases and ultimately causes a shockwave intensity of which increases with increasing angle of divergence at the upper surface. This shockwave is the same as the sudden pulse in pressure coefficient diagrams. With slight deformations, the shockwave intensity is very small and it is not possible to set a specific limit for changes in flow characteristics such as temperature, density or velocity, but as deformation becomes more significant, its intensity also increases. In addition, as the intensity of the deformation of the shockwave generated backwards increases, the "escape edge" is swept and the pressure coefficient plots show very little of it, so that at slight deformation the shockwave is in 0.4 chord whereas at detectable deformation, it is driven to 0.5 chord.

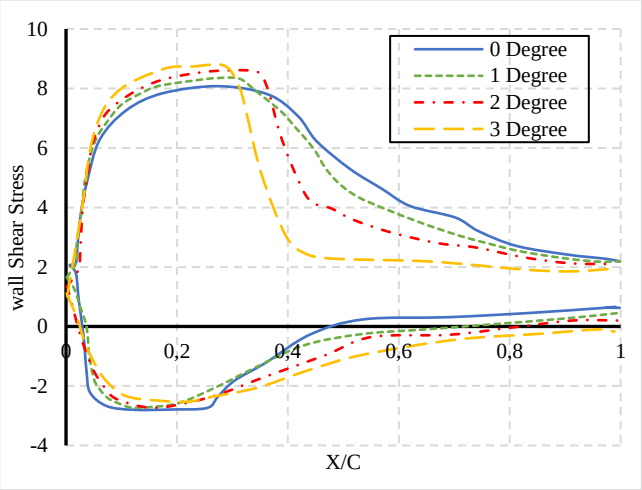

(a)

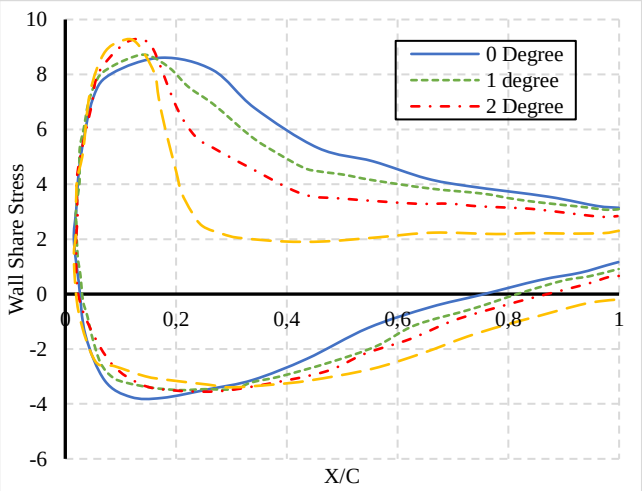

(b)

Figure 6 Wall Shear stress diagram at 2 Mach (a) SC36210 elastic airfoil, (b) NACA0018 elastic airfoil

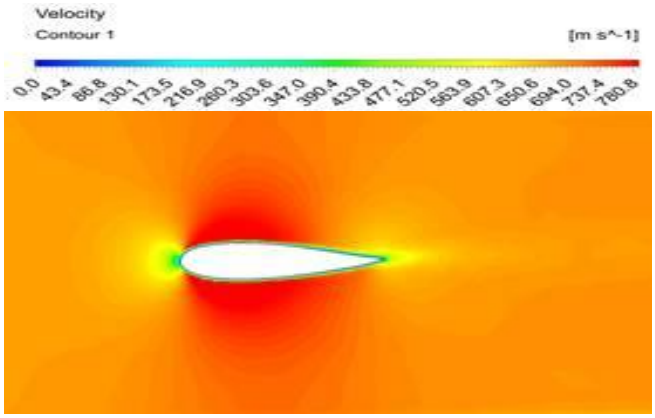

(a)

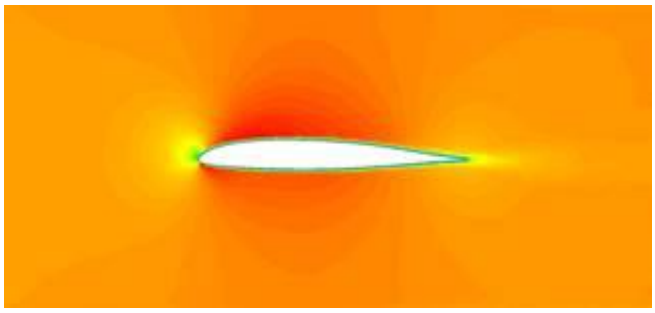

(b)

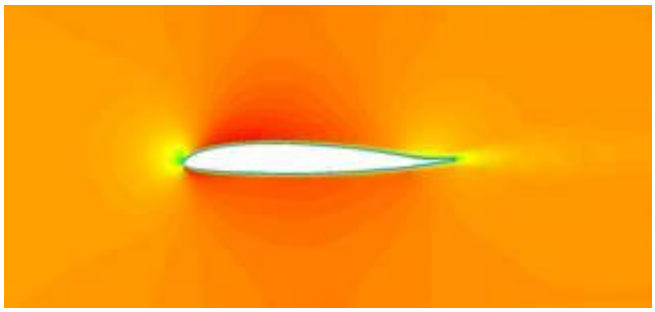

(c)

Figure 7 Velocity contours a) NACA0018-0 degrees b) NACA0018-4 degrees c) SC36210-0 degrees d) SC36210-4 degrees

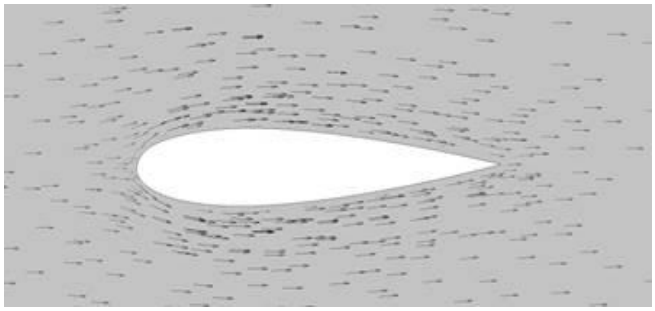

(a)

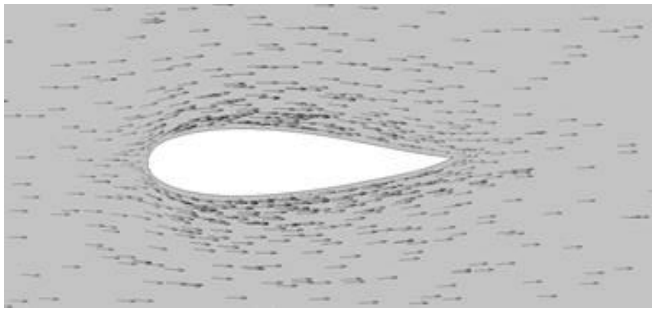

(b)

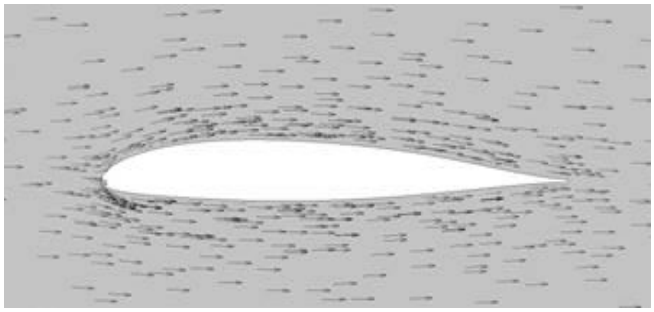

(c)

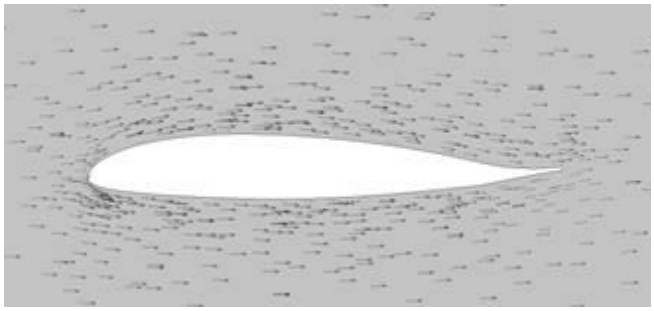

(d)

Figure 8 Velocity vectors a) NACA0018-0 degrees b) NACA0018-4 degrees c) SC36210-0 degrees d) SC36210-4 degrees

It is worth noting that the above velocity contours and vectors are for a flight with a small attack angle. However, when deformed airfoil contours are compared with rigid airfoil profile, it can be seen that, at 4-degree angle, the separation area due to deformation is more limited and that the flow stability increased in comparison to rigid state.

5. Conclusions

In this study, analyses were made using the ANSYS program. aerodynamic performance of elastically deformable airfoil profiles in the chord direction have been examined and the results were compared with rigid airfoils. This study includes two different wing three divergence angles.

Analysis of the results obtained from the aerodynamic parameters showed that the aerodynamic performance of the aircraft increased owing to the elastic deformation of the airfoil and the flight conditions for the flight were greatly improved. In this study, the best case, with optimum aerodynamic properties, was determined by examining different divergence.

According to these results, slight deformation is the best form of deformation and has strength compared to moderate and concrete deformations in terms of sequential ratio, flow separation and pressure changes. Therefore, excessive deformation in the beam direction destroys the optimal performance of the elastic airfoil and ultimately all aerodynamic properties optimized for the airfoil can be neglected.

Acknowledgments

The authors have received no funding from any person or institution.

Declaration of Conflict of Interest

The authors have no relevant financial or non-financial interest to disclose. The authors have no competing interest to declare that are relevant to the content of this article.

Author Contributions

All authors contributed to the concept and design of the study. Investigation, literature survey and data curation was carried out jointly by all authors. The numerical analysis was performed by Mansur Mustafaoğlu. The results were discussed and the first draft was written jointly by all authors. Final writing, reviewing and editing was performed by Muhammet Kaan Yeşilyurt. All authors read and approved the final manuscript.

Consent for Publication

All authors have agreed with the content of this paper and has given explicit consent for the publication of the study.

References

[1] Du S, Ang H. Design and feasibility analyses of morphing airfoil used to control flight attitude. *Strojniški vestnik-Journal of Mechanical Engineering* (2012) **58**(1):46–55.

[2] Dileep E, Nebish M, Loganathan V. Aerodynamic Performance Optimization of Smart Wing Using SMA Actuator. *Research Journal of Recent Sciences* (2013) **2277**:2502.

[3] Combes TP, Malik AS, Bramesfeld G, McQuilling MW. Efficient fluid-structure interaction method for conceptual design of flexible, fixed-wing micro-air-vehicle wings. *AIAA Journal* (2015) **53**(6):1442–1454.

[4] *Morphing trailing edges with shape memory alloy rods* (2010).

[5] Şahin HL, Yaman Y. Synthesis, Analysis, and Design of a Novel Mechanism for the Trailing Edge of a Morphing Wing. *Aerospace* (2018) **5**(4):127.

[6] Barbarino S, Bilgen O, Ajaj RM, Friswell MI, Inman DJ. A review of morphing aircraft. *Journal of intelligent material systems and structures* (2011) **22**(9):823–877.

[7] Fincham JH, Friswell MI. Aerodynamic optimisation of a camber morphing aerofoil. *Aerospace Science and technology* (2015) **43**:245–255.

[8] Yates Jr EC. *AGARD standard aeroelastic configurations for dynamic response I-Wing 445.6* (1988).

[9] Susuz U. *Aeroelastic analysis of an unmanned aerial vehicle* (2008).

[10] Liu F, Cai J, Zhu Y, Tsai HM, Wong AS. Calculation of wing flutter by a coupled fluid-structure method. *Journal of Aircraft* (2001) **38**(2):334–342.

[11] *Comprehensive Simulation Evaluation of the AGARD 445.6 Weakened Model# 3 from a Test and Evaluation Perspective* (2015). 0251 p.

[12] Vigneshwaran G, Vijayaraghavan M, Sivamanikandan K, Keerthana K, Balaji K. Fluid-Structure Interaction Over an Aircraft Wing. *Bd* **13**:27–31.

[13] Goud TS, Kumar AS, Prasad SS. *Analysis of fluid-structure interaction on an aircraft wing*: Analysis (2014).

[14] Khalaji MN, Aliihsan K, Kotcioğlu İ. Investigation of numerical analysis velocity contours k-ε model of RNG, standard and realizable turbulence for different geometries. *International Journal of Innovative Research and Reviews* (2019) **3**(2):29–34.

[15] Fincham JH, Friswell MI. Aerodynamic optimisation of a camber morphing aerofoil. *Aerospace Science and technology* (2015) **43**:245–255.

[16] Sahu S, Nourani V, Shanker U, Shanker R, Kumari V, Bansal KK, et al. Dr. Shiv K Sahu.

[17] Xie X, Cao L, Huang H. Thickened boundary layer theory for air film drag reduction on a van body surface. *AIP Advances* (2018) **8**(5):55129.

[18] Tay WB, Lim KB. Numerical analysis of active chordwise flexibility on the performance of non-symmetrical flapping airfoils. *Journal of Fluids and Structures* (2010) **26**(1):74–91.

[19] Pederzani J, Haj-Hariri H. Numerical analysis of heaving flexible airfoils in a viscous flow. *AIAA Journal* (2006) **44**(11):2773–2779.

[20] Bazilevs Y, Takizawa K, Tezduyar TE. *Computational fluid-structure interaction: methods and applications*: John Wiley & Sons (2013).

[21] Donea J, Huerta A, Ponthot JP, Rodríguez-Ferran A. *ch 14*: Wiley New York (2004). p. 1–25.

[22] Benra F-K, Dohmen HJ, Pei J, Schuster S, Wan B. A comparison of one-way and two-way coupling methods for numerical analysis of fluid-structure interactions. *Journal of applied mathematics* (2011) **2011**.